Structure Changes during Uniaxial Deformation of Ethylene-Based Semicrystalline Ethylene−Propylene Copolymer. 1. SAXS Study

Li-Zhi Liu,[†,§] Benjamin S. Hsiao,[*,†] Bruce X. Fu,[†] Shaofeng Ran,[†] Shigeyuki Toki,[†] Benjamin Chu,[†] Andy H. Tsou,[‡] and Pawan K. Agarwal[‡]

Department of Chemistry, State University of New York at Stony Brook, Stony Brook, New York 11794-3400, and ExxonMobil Chemical Company, Baytown Polymers Center, Baytown, Texas 77522-5200

Received May 20, 2002

ABSTRACT: In-situ structural changes at the lamellar level during uniaxial deformation and subsequent relaxation of a semicrystalline ethylene−propylene (EP) copolymer containing 78 wt % ethylene were studied by time-resolved synchrotron small-angle X-ray scattering (SAXS) at room temperature (25 °C). During the initial stage of deformation, the long period was found to increase in the stretching direction and decrease in the transverse direction. In addition to the elastic change of the lamellar structure, further analysis suggested that there was an additional contribution of strain-induced "melting", which began at a relatively low strain (about 10%) and was directionally dependent. At 75% strain, new crystals, possibly with extended-chain conformation and needlelike microvoids, started to form, which coexisted with the original crystals (dominated by folded-chain conformation). Because of the destruction of original crystals, the applied stress was found to decrease slightly after the yield point. Above 120% strain, the stress increased linearly with strain partially due to the formation of new crystals. Long periods of new crystals decreased with strain upon further stretching. During relaxation, a large amount of well-oriented new crystals remained in the sample. As a result, only 55% of the original sample length was recovered. The long period of the new crystals after relaxation was about 15 nm, much smaller than that of the original crystals (24 nm). Strain-induced microvoids were also found to remain in the sample after relaxation.

Introduction

Since the introduction of ethylene−propylene rubber, or EPM by ASTM designation, in the early 1960s, it has been one of the fastest growing elastomers[1] for its excellent ozone resistance and high extensibility. Here, E stands for ethylene, P stands for propylene, and M represents the polymethylene type backbone. Ethylene−propylene copolymers are solution polymerized using soluble Ziegler−Natta catalysts. EPM polymers with higher ethylene contents contain some crystallinity from the ethylene segments. The ethylene crystallinity depends on the ethylene content and sequence distribution along the polymer chains.[2] Crystallinity provides enhanced mechanical strengths, better extrusion properties, allows higher filler and oil loading capabilities, and easier pelletization processes. During deformation, these polymers yield and undergo further crystallization.[3] Although yielding leads to permanent dimensional changes after the first extension, the recovery properties upon second and further extensions resemble those of chemically cross-linked rubbers fairly well. Recently, with advancements in the metallocene catalyst techniques, semicrystalline ethylene−octene elastomers with densities less than 0.89 g/cm^3 have been prepared.[4] Elastic properties of these ethylene−octene copolymers were attributed to the presence of fringed-micelle-like crystals in high-octene content copolymers.[5]

High ethylene content EPM and polyethylene (PE) homopolymers contain the same crystallizable ethylene segments in the main chains. However, the observed crystalline structures in EPM and PE are quite different. A pseudohexagonal structure, instead of the conventional orthorhombic structure in PE,[6] has been reported by Ballesteros et al.,[7] based on static wide-angle X-ray diffraction (WAXD) measurements on oriented semicrystalline EPM. Additionally, several studies on the structure, property, and process relationships in semicrystalline EPM have been reported.[8−10] Guerra et al.[8] and Kolbert et al.[9] examined the structure and corresponding properties of several EPM copolymers whereas Mathot et al.[4] have carried out time-resolved simultaneous synchrotron small-angle X-ray scattering and wide-angle X-ray diffraction (SAXS/WAXD) investigations of EPM polymers in combination with differential scanning calorimetry (DSC). However, none of these studies have addressed morphological and concurrent property changes of EPM during mechanical deformation.

Understanding of the crystalline structural developments in EPM polymers at the molecular and lamellar levels during deformation, and the resulting impacts on elastic properties, is essential in EPM material design for practical applications. It needs to be pointed out that in-depth deformation studies are quite abundant in other thermoplastic elastomers, such as polyurethanes (PU).[11−17] In the present study, the in-situ SAXS technique using synchrotron radiation in combination with a tensile stretching apparatus was carried out to obtain mechanical and structural information during uniaxial deformation and relaxation of an EP elastomer containing 78 wt % ethylene. Results from the in-situ

[†] State University of New York at Stony Brook.
[‡] ExxonMobil Chemical Company.
[§] Current address: The Dow Chemical Company, 2301 Brazosport Blvd. B-1470, Freeport, TX 77541-3257.
* To whom correspondence should be addressed. E-mail bhsiao@notes.cc.sunysb.edu.

10.1021/ma020771i CCC: $25.00
Published on Web 03/01/2003

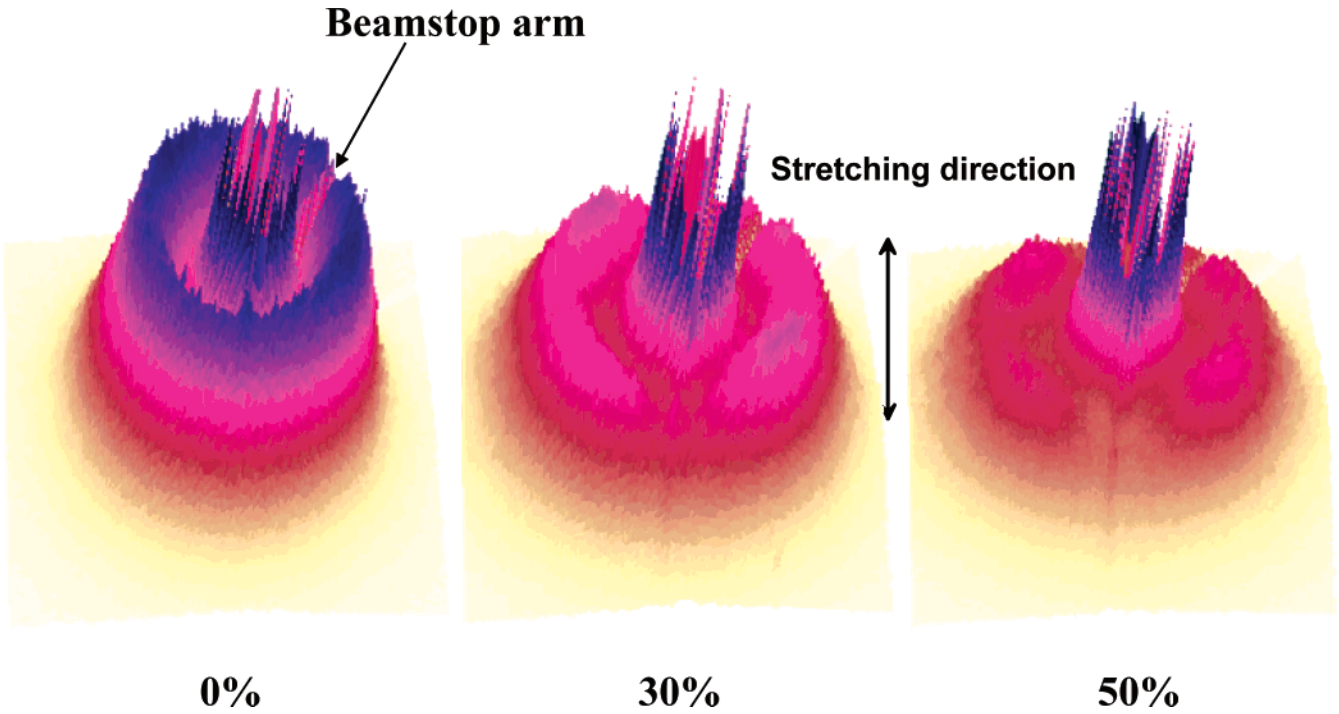

Figure 1. 3-Dimensional SAXS patterns of semicrystalline EP copolymer at strains from 0 to 50%.

WAXD study of the same sample will be presented later.

Experimental Section

The selected EP copolymer was a sample made by Exxon-Mobil Chemical Co. It was synthesized with a conventional vanadium catalyst and had molecular weights $M_n = 7.6 \times 10^4$ g/mol and $M_w = 1.7 \times 10^5$ g/mol. This polymer contains 78 wt % ethylene and has a maximum degree of crystallinity of about 20% (determined by differential scanning calorimetry, DSC, at a 10 °C/min heating rate). This polymer was melt-pressed at 180 °C into a film of 1 mm thickness and was then rapidly cooled to room temperature. The rapid cooling process did not significantly change the 20% crystallinity. All specimens were cut into rectangular strips of $0.1 \times 1 \times 6$ cm^3 dimensions. Time-resolved SAXS and wide-angle X-ray diffraction (WAXD) experiments were performed at the Advanced Polymers Beamline (X27C), National Synchrotron Light Source (NSLS), and Brookhaven National Laboratory (BNL). The wavelength used was 0.137 nm. A three-pinhole collimation system was used to define the incident beam from a double multilayer monochromator. The sample-to-detector distance for the SAXS study was 1600 mm. The collected SAXS images were calibrated with the silver behenate standard. A MAR-CCD (MAR USA, Inc.) two-dimensional detector was used for the real-time data collection. The typical image acquisition time was 15 s per image. The observed images were only corrected for beam fluctuations.

The deformation of the sample was performed with a modified Instron 4442 tensile apparatus. The original length between the Instron jaws was 30 mm. The stretching was carried out in a symmetrical mode, where the detection spot on the sample remained fixed in space. The experiments were carried out at room temperature (25 °C). A constant extension rate (10 mm/min) was applied to the specimen throughout the deformation process. The SAXS images were taken immediately after the desired strain value was reached during either the deformation process or the relaxation process.

Results and Discussion

Structure Changes at Small Strains. Crystalline structure development at the lamellar level during uniaxial deformation of the EP copolymer was investigated by two-dimensional (2D) synchrotron SAXS. Selected SAXS patterns collected at small strains (up to 0.5) are shown in Figure 1. In the undeformed sample, an isotropic scattering ring was observed. This ring resulted from the lamellar structure containing alternating ethylene crystalline lamellae and EP amorphous chains; the structure had no preferred orientation. The long period L, representing the average distance between the adjacent crystalline lamellae, could be determined from the position of the scattering peak q^* using Bragg's law $L = 2\pi/q^*$, where $q = 4\pi/\lambda \sin(\theta)$ with λ being the wavelength and 2θ being the scattering angle. A long period of about 24 nm was found in the undeformed sample. During stretching, the SAXS pattern changed dramatically with strain, as shown in Figure 1. At 30% strain, an anisotropic SAXS pattern having an elliptical scattering background, where the long axis was perpendicular to the stretching direction, and four scattering peaks, evenly distributed in each quadrant, were seen. The total integrated intensity (proportional to the invariant) decreased about 50% at this stage. At 50% strain, the four-point pattern became very distinct and the elliptical background diminished substantially. The total integrated intensity of the pattern at 50% strain was only about 25% of that of the initial pattern; i.e., the total integrated intensity decreased about 75%.

The appearance of elliptical scattering at 30% strain indicated that the long period of the adjacent lamellae in the stretching direction was larger than that in the transverse direction.This could also be seen by the linear scattering profiles taken along the two principal axes. Figure 2a illustrates the SAXS profiles in the stretching direction, where the scattering peak is found to shift to a lower q value with increasing strain, indicating the increase of the long period. The calculated results showed that the long period in the stretching direction increased from 24 to 30 nm (i.e., 25% change) at the strain of 30%. Figure 2b illustrates the scattering profiles perpendicular to the stretching direction. The scattering peak was found to move to a higher q value—

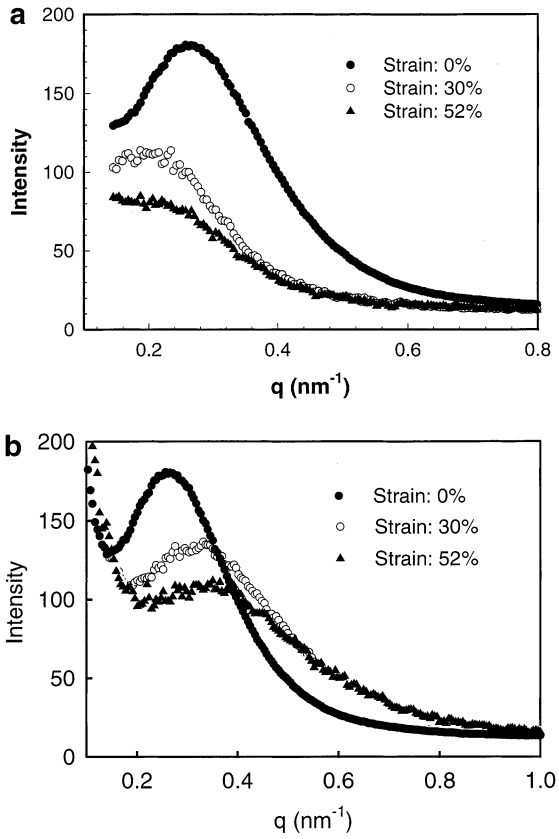

Figure 2. Linear SAXS profiles at different strains (a) in stretching direction and (b) in the equatorial direction.

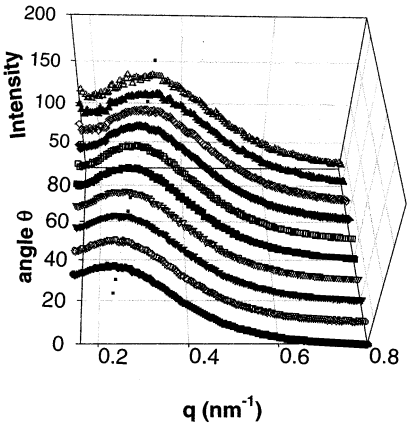

Figure 3. Linear SAXS profiles at different azimuthal angles ($\phi = 0°$ represents the stretching direction); data taken from the 2D SAXS pattern at strain = 30%.

the long period decreased from 24 to 19 nm (i.e., about 20% change) at a strain of 30%. Figure 3 shows a series of scattering profiles at 30% strain taken at various azimuthal angles ϕ from the 2D SAXS pattern. The long period was found to change continuously in different directions. In Figure 3, $\phi = 0°$ represented the stretching direction and $\phi = 90°$ represented the equatorial direction. It was seen that the position of the scattering peak (corresponding to the long period) changed continuously with respect to the azimuthal angle. However, from the intensity scale in Figure 2, we also noted that the scattered intensities at 30% strain decreased quite substantially from that of the undeformed sample. Combined observations of the near elastic change in the long period and the drastic decrease in total scattered intensity indicated that two events probably occurred

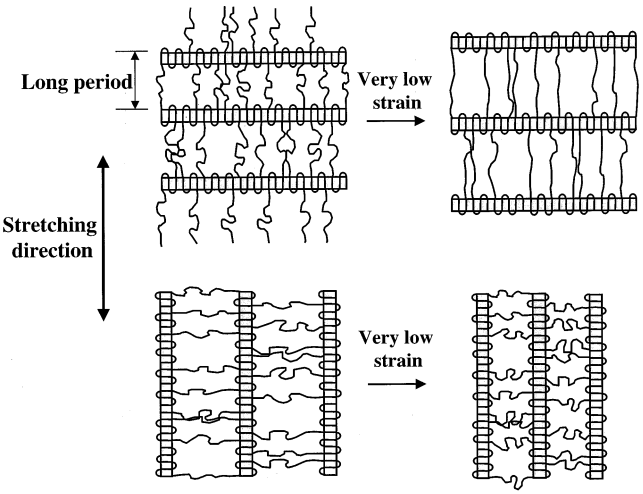

Figure 4. Schematic diagram of the elastic deformation (at very low strains) in lamellae aligned along and perpendicular to the stretching directions.

concurrently during the deformation stage even of low strains. These events included (1) affine deformation of the lamellar structures and (2) destruction of some lamellar crystals.

The scheme for affine deformation of the lamellar structure in EP copolymer at small strains can be understood as follows. Figure 4 illustrates the elastic changes of the lamellar structure in two extreme orientations: (1) the lamellar stack parallel to the stretching direction and (2) the lamellar stack perpendicular to the stretching direction. The initial lamellar structure contains stacks of thin lamellae (with thickness no more than 20% of the long period because of 20% crystallinity). The crystalline lamellae are probably dominated by the folded-chain conformation. The tensile deformation enlarges the average spacing of the lamellae oriented perpendicularly to the stretching direction, while it contracts the lamellae oriented parallel to the stretching direction. If we assume that there is no structural transition, such as melting or crystallization, at low strains, this EP polymer can be considered as an elastic rubber with a Poisson's ratio of 0.5. However, considering that the crystal lamella have higher modulus than that of the amorphous chain, the final moduli of the lamellae assembly must be directional dependent. Thus, as the perpendicularly aligned lamellar assembly elongates due to the lower modulus of the amorphous layer, the parallel-aligned lamellae are expected to contract in accordance with the isovolume constraint imposed by the amorphous region. The long period change of the lamellar stacks with in-between orientations should be bounded by these two limitations. Later, we will demonstrate results that only at strains less than 10%, the lamellar structure change in the chosen EP copolymer is elastic.

The affine deformation cannot account for the large decrease in the integrated scattered intensity (e.g., scattered intensity decreased about 50% at 30% strain). We note that although deformation can increase the density of some amorphous chains (as seen in the lower right diagram in Figure 4), thus decreasing the scattering contrast (scattering invariant is proportional to the square of the density contrast, the difference between the densities of the crystalline lamellae, and the amorphous layer), it can also decrease the density of some amorphous region (the upper right diagram in

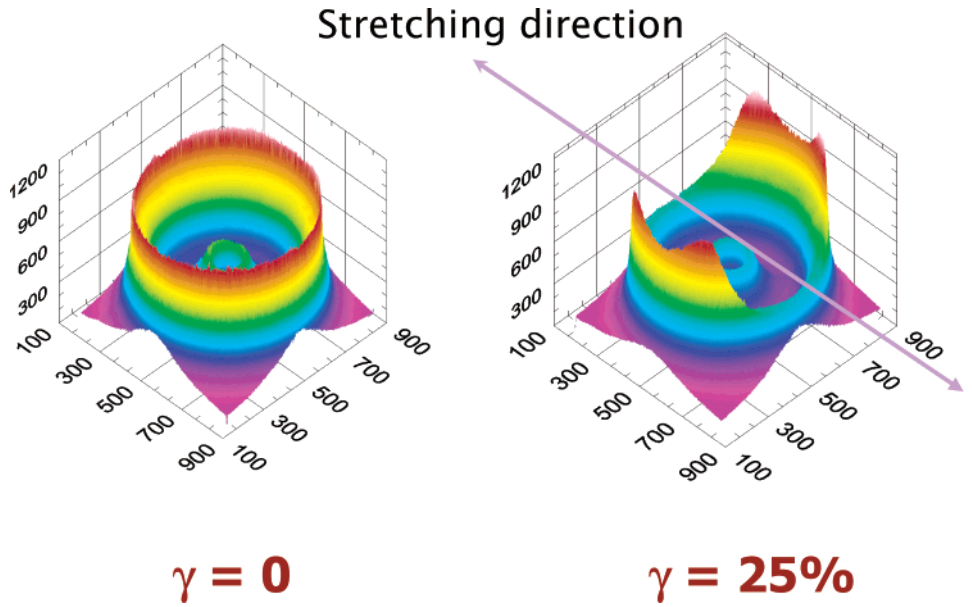

Figure 5. 3-Dimensional WAXD patterns of semicrystalline EP copolymer at strains of 0 and 25%. The dominant diffraction peak coincides with the (110) reflection from the orthorhombic unit cell of PE crystals.

Figure 4), thus increasing the scattering contrast. These two effects should more or less offset each other and leave the integrated intensity unchanged. However, this was not seen, which suggested that a fraction of the crystalline structure must be destroyed by deformation.

Strain-Induced Melting. We chose the phrase "strain-induced melting" to describe the annihilation or the destruction of some crystalline entities during deformation. However, SAXS results alone were not sufficient to support this argument since the scattered intensity is not directly related to the crystallinity. The strain-induced melting process was further verified by a separate in-situ wide-angle X-ray diffraction (WAXD) study under the same deformation conditions. Two selected WAXD images (after normalization of beam fluctuation) of the EP copolymer under stretching are shown in Figure 5. In this figure, the left WAXD image represents the (isotropic) diffraction pattern at the undeformed state; the right image represents the diffraction pattern collected at strain of 0.25 (low strain). The observed dominant diffraction peak coincides with the (110) reflection from the orthorhombic unit cell of PE crystals. It was seen that the stretching process, even at a low strain value (0.25), significantly reduced the diffraction intensity along the machine direction (i.e., the meridional direction, assuming a fiber symmetry), while the diffraction intensity profile perpendicular to the stretching direction was rearranged (the maximum intensity appeared at four off-axis positions) but the corresponding intensity was not increased. The large intensity drop along the stretching direction cannot be explained by the missing intensity due to flat plate detection from an oriented sample, as the rule will apply only for the (00*l*) reflections, not for the (*hk*0) reflection. Therefore, the notable overall intensity decrease of the (110) reflection was consistent with the loss of crystallinity, which supports the process of strain-induced melting. The exact nature of the changes in crystal orientation, crystal structure, and crystallinity will be discussed later in a different paper.

The behavior of strain-induced melting became more evident in the SAXS patterns obtained at higher strains. Figure 6 shows a distinct four-point scattering pattern at 74% strain. At 88% strain, the intensity of the four-point scattering decreased, whereas two additional weak scattering peaks began to appear in the stretching direction. After a further increase in strain to 103%, the four-point scattering pattern was reduced to two blurred scattering arcs on the equator, while the intensity of the newly developed scattering peaks in the stretching direction was found to increase.

The appearance of the four-point pattern and its conversion to the two-arc pattern on the equator resulted from the unique pathway of the strain-induced melting process at intermediate strains, which could be understood as follows. The four-point pattern in Figure 6 is directional dependent. Figure 7 illustrates selected linear scattering profiles at different azimuthal angles (ϕ) taken from the 2D SAXS pattern at 74% strain. It was seen that the scattered intensity exhibited a weaker shoulder at azimuthal angles between 0° and 50° (ϕ = 0° is the stretching direction), a distinct peak at ϕ = 70°, and an intermediate peak at ϕ = 90° perpendicular to the stretching direction. The weak scattered intensity at ϕ = 0° suggested that the lamellar stacks perpendicular to the stretching direction were largely destroyed, while the intermediate scattered intensity at ϕ = 90° suggested that some fractions of the lamellar stacks parallel to the stretching direction were preserved. The above findings indicated that the melting (or destruction) process in lamellae induced by strain must also be directionally dependent. Apparently, the lamellar stacks perpendicular to the stretching direction melted first. This hypothesis was also consistent with results in Figure 6, in which the azimuthal angle of the peak position in the four-point pattern was not constant—it shifted toward the equator with increasing strain. Furthermore, the peak position moved toward the beam center (lower q values) at higher strains, indicating an increase in the long period. The long period rise was consistent with destruction of some lamellar, which resulted in the increase in the average distance between the remaining lamellae.

The appearance of the four-point SAXS pattern can be explained by the pathway of the strain-induced melting process, as shown in Figure 8. The top diagram

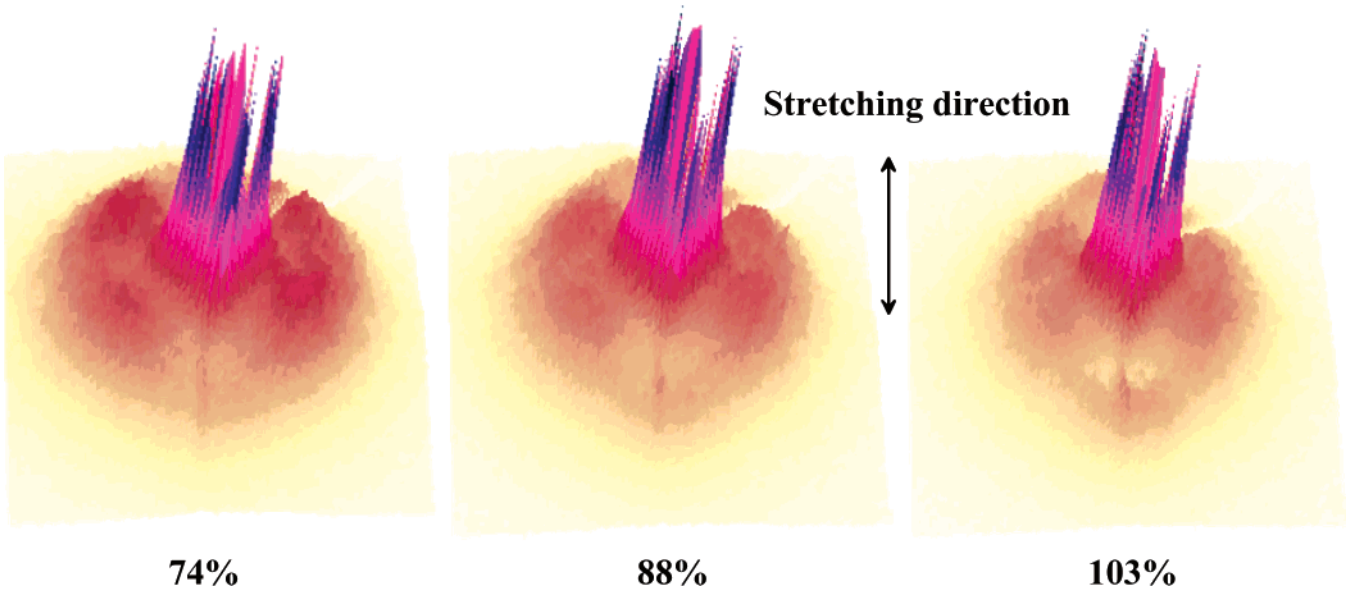

Figure 6. 3-Dimensional SAXS patterns of semicrystalline EP copolymer at strains from 74 to 103%.

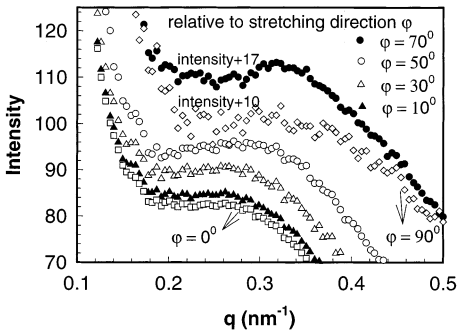

Figure 7. Linear SAXS profiles at different azimuthal angles ($\phi = 0°$ represents the stretching direction); data taken from the 2D SAXS pattern at strain = 74%.

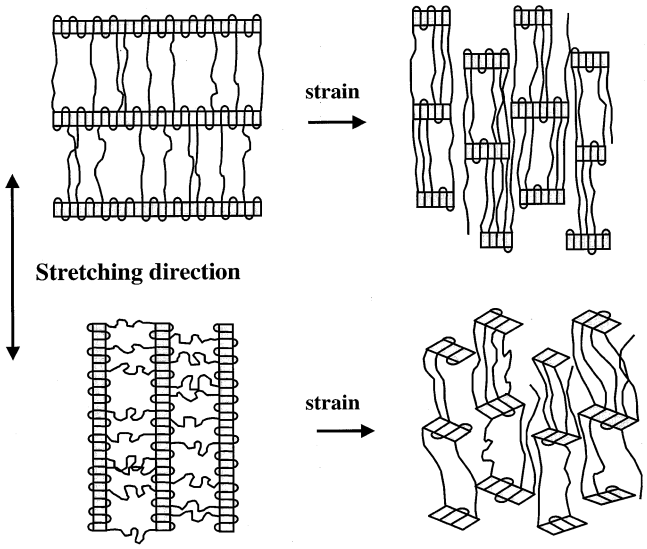

Figure 8. Schematic diagram of the strain-induced melting (crystal destruction) in lamellae aligned along and perpendicular to the stretching directions.

illustrates the lamellar stacks aligned perpendicular to the stretching direction. At sufficiently large strains, the local stress of some extended amorphous chains would exceed the crystal binding force, resulting in chain pullouts and disintegration of the lamellae. The resulting morphology can thus become an assembly of smaller lamellar blocks having a checkerboard arrangement to minimize the stress concentration. This morphology has been observed in many semicrystalline polymers under deformation[18] and is consistent with the observed four-point SAXS pattern in this study. In another scenario, where the lamellar stacks are aligned parallel to the stretching direction, the increase in strain will also cause the disintegration of the lamellae, as shown in the bottom diagram of Figure 8. At high strains, the stress on the amorphous chains that are perpendicular to the lamellar axis would tend to reorient in the stretching direction. If the local stresses of the chains can overcome the crystal binding energy, the lamellae would not only be disintegrated into smaller blocks but also be rotated in order to alleviate the stress concentration. The resulting morphology would be an assembly of tilted lamellae having a checkerboard arrangement. The degree of tilting is dependent on the applied strain. Such morphology will also produce a four-point pattern in SAXS. Of course, if the orientation of the lamellae stacks is between these two cases, the resulting morphology will also be in between these two extremes. The observed four-point pattern in SAXS thus represents the superposition of the checkerboard morphology containing small lamellar blocks of different orientations.

Strain-Induced Crystallization. Another important feature of the structure change induced by stretching is the strain-induced "crystallization" (or recrystallization). Figure 6 shows that two new scattering bars, being related to the formation of strain-induced crystals, appear in the stretching direction at 88% strain. This behavior can be examined further by plotting the linear scattered intensity profiles in the stretching direction at different strains using the data in Figure 6. In Figure 9, the scattering profile at 74% strain began to exhibit a scattering shoulder at $q \sim 0.27$ nm^{-1} ($d = 23$ nm) due to the new crystals and a weak scattering peak at $q \sim 0.21$ nm^{-1} ($d = 30$ nm) due to the original crystals. The smaller long period in the newly formed crystalline structure suggested that the topology of the strain-induced crystalline network was much denser than that of the initial crystalline network.

The SAXS patterns collected at higher strains (118−190%) are shown in Figure 10. At 118% strain, the SAXS pattern was dominated by the two-bar pattern

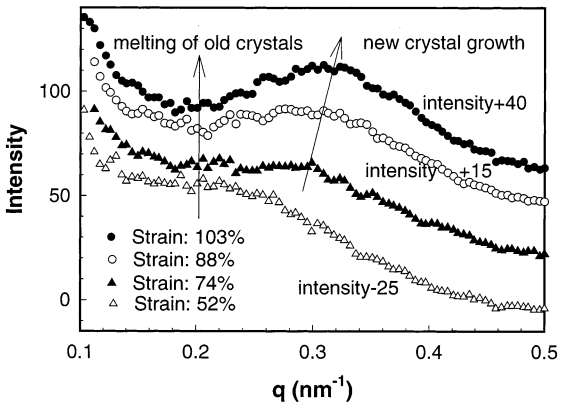

Figure 9. Linear SAXS profiles in the stretching direction at strains from 52 to 103%.

in the stretching direction, while the original four-point scattering was reduced to two weak scattering shoulders on the equator. At higher strains (158% and 190%), only the two-bar pattern was seen. The meridional two-bar pattern resulted from the morphology of newly developed strain-induced crystals. The population of the new crystals grew with increasing strain, which was evident by the progressive increase of the scattered intensity. From Figures 6 and 10, it was seen that both new crystals and original crystals coexisted at strains between 74% and 118%. Above the strain of 118%, all original crystals disappeared. Although not shown here, we have also carried out experiments with strains up to 650%, where the two-bar scattering feature was found to remain about constant, suggesting that the newly developed lamellar structure was stable at high strains until break.

The crystallization of this copolymer under no deformation is probably dominated by folded-chain conformation, while the strain-induced crystals formed at higher strains (>0.7) are probably dominated by extended-chain conformation. A schematic diagram of the lamellar structures from the initial folded-chain crystal dominant stack (undeformed) and the extended-chain crystal dominant stack (at higher strains) is illustrated in Figure 11. The well-oriented two-bar scattering pattern at high strains implied that the newly developed extended-chain crystal lamellae were aligned perpendicular to the stretching direction. The corresponding long period at each strain value could be obtained from the scattering profiles shown in Figure 12. The long period of the newly developed strain-induced crystals was 20 nm (at strains from 1.03 to 1.58), which was smaller than that (24 nm) of the original lamellar stacks at zero strain and significantly smaller than that (30 nm) of the deformed lamellar stacks at 30% strain during elastic deformation. The long period continued to be 20 nm at strains ranging from 103% to 158%, as shown in Figure 12. However, the long period was found to decrease to 18 nm when the strain was increased from 158% to 190%, indicating that more new crystals were generated in the stretching direction. At higher strains, no substantial change in the long period value was seen. In Figure 12, the peak intensity was found to increase with increasing strain from 118% to 190%. (We note that the intensity in Figure 12 was not corrected for the change in thickness; the intensity increase after the volume correction was quite substantial.) The scattered intensity increase was consistent with the notion that more strain-induced crystals were formed and aligned in the stretching direction at high strains. The above SAXS study indicated that the major structural changes at the lamellar level took place within the strain range of 0−200%.

Structure Change during Stress Relaxation. As deformation induces continuous structural changes (e.g., melting and recrystallization) in the EP copolymer, the behavior of structural recovery during stress relaxation was also investigated. In this study, the sample was first stretched to a strain of 190% and then allowed gradual removal of the load. SAXS measurements were carried out during stress relaxation. The engineering stress−strain curve during the stretching and recovery processes is shown in Figure 13, which can be related to structural changes and will be discussed in the next section. Three selected SAXS scattering patterns are shown in Figure 14 during the recovery process, exhib-

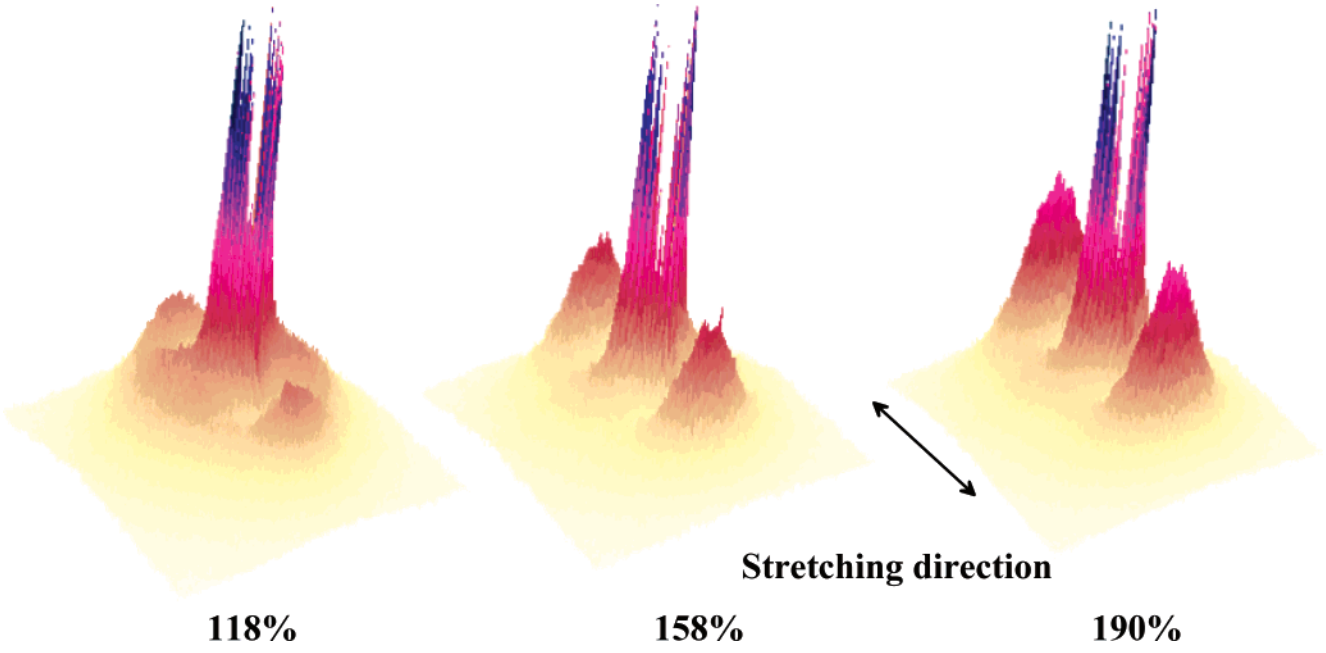

Figure 10. 3-Dimensional SAXS patterns of semicrystalline EP copolymer at strains from 118 to 190%.

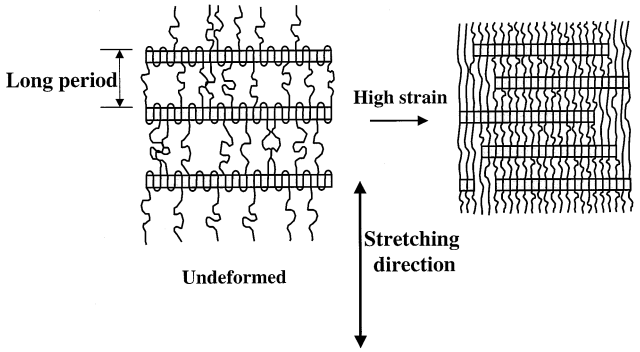

Figure 11. Schematic diagram of the lamellar structures from the folded-chain crystal dominant stacks (undeformed) and the extended-chain crystal dominant stacks (at high strains).

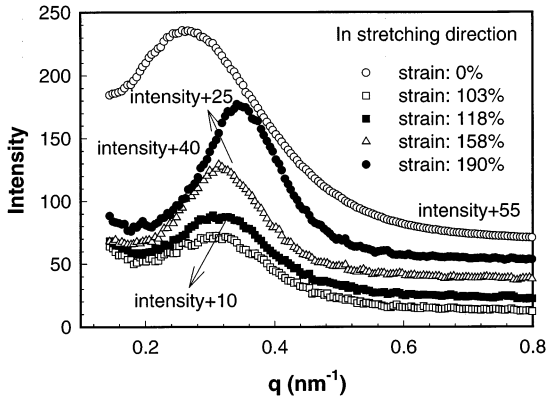

Figure 12. Linear SAXS profiles in the stretching direction at strains from 103 to 190% (the profile at strain = 0 is included as a reference).

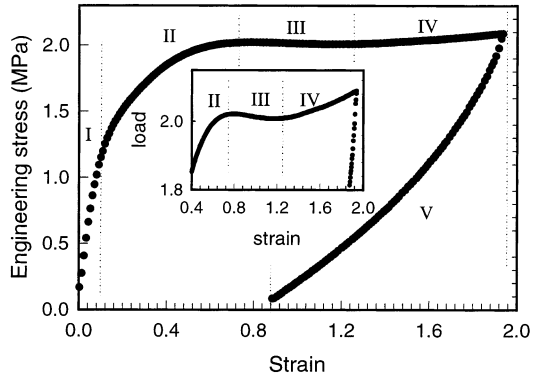

Figure 13. Engineering stress−strain curve during stretching and recovery processes (the maximum applied strain was 190%).

iting several unique features: (1) the two-bar pattern remains during the recovery process even when the stress becomes zero, (2) the intensity of the two-bar pattern decreases with the decrease in strain, and (3) a weak four-point pattern appears when the stress is removed. In the last case (load free), the four-point pattern is superimposed on the stronger two-bar pattern, making the total scattering pattern look like a number "8". From (1) and (2), we conclude that a large fraction of the strain-induced crystals are thermally stable at room temperature. The majority of these crystals can maintain both dimensional and orientational stability even when the stress is removed. However, the rest of the strain-induced crystals cannot maintain the orientation and are relaxed into some tilted positions after stress removal. Linear scattered intensity profiles taken along the stretching direction of the SAXS patterns (Figure 14) are plotted in Figure 15, where the peak position was found to shift to higher q values during the recovery process. The peak shifting indicated a decrease in the long period during the recovery process. The changes in the long periods during both stretching and recovery processes are plotted against strain in Figure 16. It was seen that the long period in the stretching direction increased with strain up to the value of 30%, which supported the occurrence of strain-induced melting as verified by WAXD (Figure 6). When strain-induced crystallization began, the long period value fell noticeably (to about 20 nm at the strain range from 88% to 190%). The decrease in the long period at strains between 60% and 80% resulted from the melting of original crystals with a large long period (30 nm) and the growth of newly developed crystals with a small long period (20 nm). During the recovery process, the long period decreased further from 18 nm at 190% strain to 15 nm at 88% strain without load. The decrease in the long period during recovery can be explained by the relaxation of stretched amorphous chains.

The weak four-point scattering pattern observed in Figure 14 (after relaxation) showed a broad angular distribution, suggesting that the relaxed crystals were rearranged into a wide range of orientation. Furthermore, a large distribution of the long period was also found from the linear intensity profiles taken at different azimuthal angles of the SAXS pattern from the relaxed sample, as shown in Figure 17. The scattering peak in Figure 17 progressively shifted to a low q value with increasing azimuthal angle. The long period in the stretching direction ($\phi = 0°$) was 15 nm. It increased to about 18 nm at $\phi = 30°$ and about 27 nm at $\phi = 50°$, implying that some lamellar assemblies with the smaller long period were stable enough to maintain the orientation in the stretching direction, while the assemblies with longer long periods (loosely packed structures) were reorientated.

From the above results, we can summarize several unique characteristics of the strain-induced crystals. (1) As crystallization occurs due to interactions of parallel stretched chains, the induced crystals must contain extended-chain conformation. (2) The morphology of strain-induced crystals shows a highly oriented "layered" structure (Figure 11). (3) The crystal dimensions of the strain-induced crystals are slightly smaller than those of the original crystals. This has been verified by the WAXD study (results to be published elsewhere), and it was also supported by the observation of the shorter long period of the strain-induced crystals than that of the undeformed sample. (4) The population of the strain-induced crystals increases with strain, as indicated by the increase in the scattered intensity of the two-bar pattern at higher strains.

Structure−Property Relationship. The mechanical property of the EP copolymer can be related to the changes in the crystalline structure and morphology. In Figure 13, the engineering uniaxial stress−strain curve is illustrated (the inset figure represents the enlarged strain scale, where the yield point—80% strain—is identified). This stress−strain curve can be divided into five regions for discussion. The first four regions represent the stretching process; the last region represents the recovery process. Region I, within the strain range of 0 and 10%, is the elastic region, where the stress of

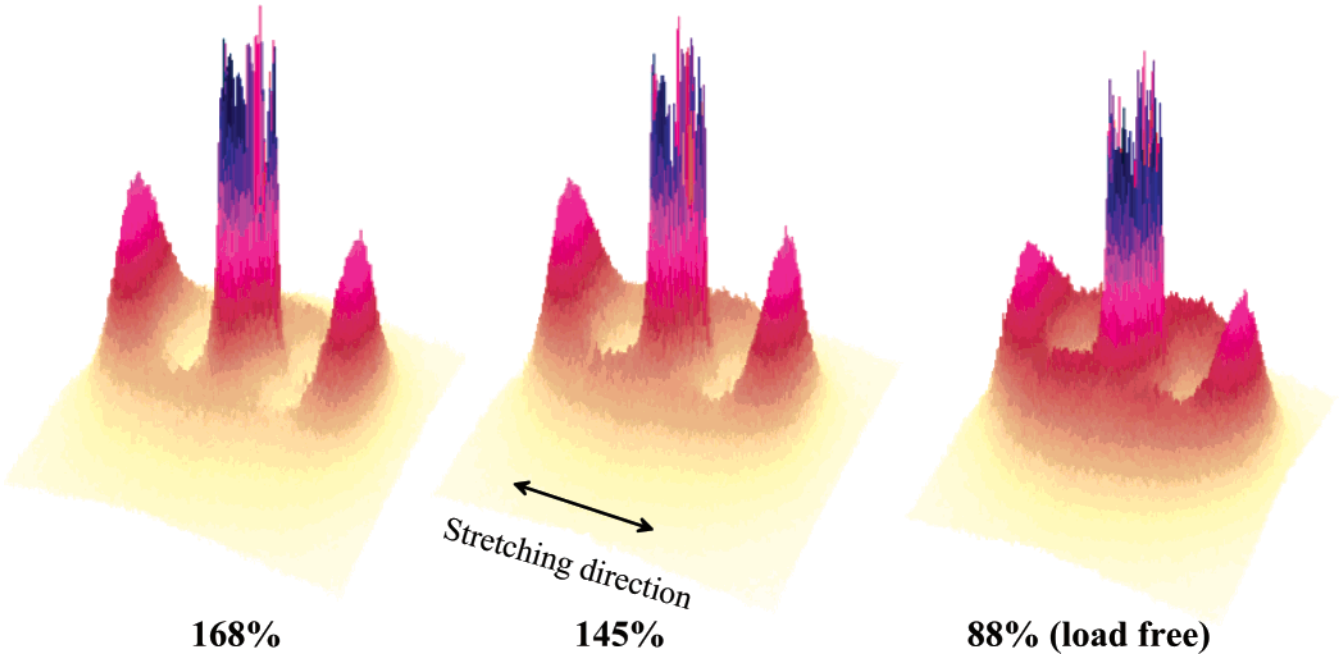

Figure 14. 3-Dimensional SAXS patterns of the stretched semicrystalline EP copolymer during the recovery process (the maximum applied strain was 190%).

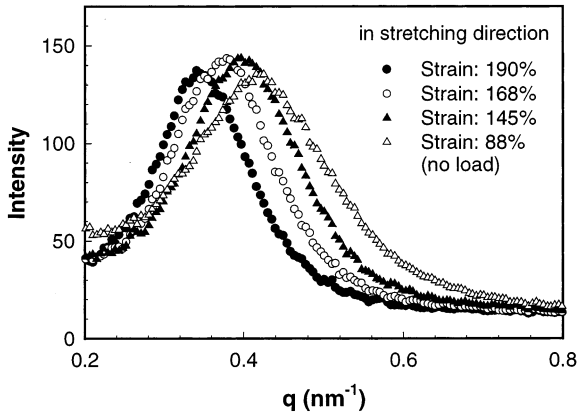

Figure 15. Linear SAXS profiles in the stretching direction during the recovery process (the maximum applied strain was 190%).

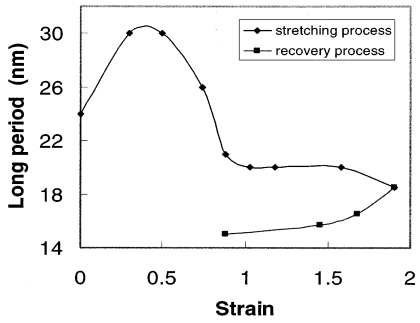

Figure 16. Long period of the copolymer in stretching direction vs strain for the stretching and recovery processes.

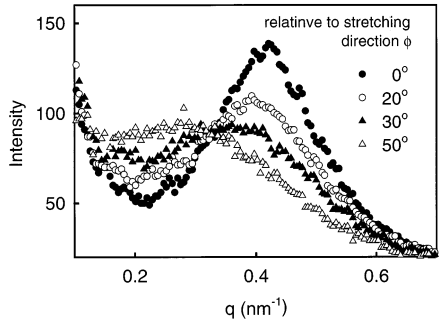

Figure 17. Linear SAXS profiles at different azimuthal angles ($\phi = 0°$ represents the stretching direction); data taken from the 2D SAXS pattern of the relaxed EP copolymer after the sample has been stretched to a strain of 190%.

the material increases nearly linearly with strain. In region II, the rate of stress increase is retarded, especially when approaching the yield point. This stress response is consistent with the decrease in the SAXS scattering power (invariant) with strain, indicating that the strain-induced melting becomes dominant. Region III ranges from 80% strain (the yield point) to 120% strain. Although the original crystals are being continuously destroyed, this region is marked by the event of strain-induced crystallization. In this region, the stress decreases with strain after the yield point is probably still dominated by the effect of melting (crystal destruction) as opposed to the process of crystal formation. In region IV (at strains above 120%), all the original crystals are melted away, and the population of new crystals continues to grow with strain. The inset of Figure 13 shows that the stress increases almost linearly with strain in region IV, and such a linear relationship between stress and strain is also seen at much higher strains (Figure 18, where the maximum applied strain was 580%). The strain-induced crystallization is the dominant effect in region IV, which is primarily responsible for linear stress−strain relationship. Region V represents the recovery process. In Figure 13, it was seen that the residual strain was 88% when the load was completely removed; this led to the recovery ratio of 55% after the first stretching. The permanent changes in structure after stretching are due to the combined processes of strain-induced melting and subsequent crystallization. In this region, a fraction of the crystals are reoriented with the decrease in stress, while the rest can retain their orientation.

The evidence of strain-induced crazes was seen from the SAXS measurements. In Figure 19, the SAXS

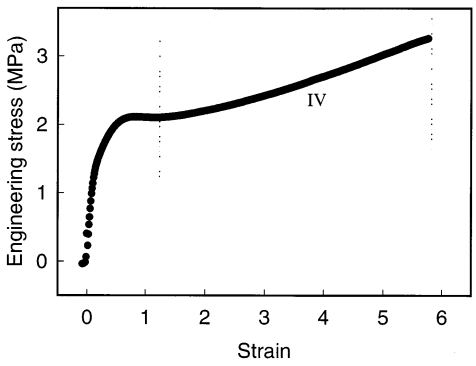

Figure 18. Engineering stress−strain curve during the stretching process at a maximum strain of 580%.

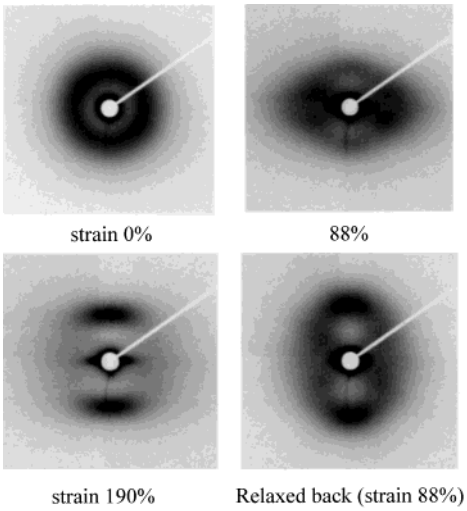

Figure 19. Selected 2D SAXS scattering patterns at different strains during the recovery process.

pattern showed a strong scattering streak (its intensity was significantly stronger than that of the two-bar pattern on the meridian) in the equatorial direction near the beam stop when the applied strain was near the yield point. The streak exhibited the fingerprint of the craze formation or development of elongated microvoids aligned along the stretching direction.[19,20] If the voids had a perfect alignment and a finite dimension, the angular width of the streak along the stretching direction should be constant at different scattering angles. However, this was not seen in any of the patterns obtained, implying that both the size distribution and the random orientation of the voids had contributed to the streak profile.[20] There was no obvious change in the appearance of equatorial streak after its formation in regions II and III, where both strain-induced melting and crystallization took place. However, in region VI, where only the crystal growth is present, the width of the streak became narrower (Figure 19 at a strain of 190%). This implied that the voids became elongated and/or were better aligned along the stretching direction. During the relaxation process, the breadth of the streak became broader, indicating that the voids were smaller and less oriented. It was noticed, however, that the streak feature persisted even when the sample was totally relaxed (Figure 19), indicating that some voids remained present in the relaxed material.

Conclusions

1. In the initial stage of the uniaxial stretching process (region I, strain less than 10%), the stress−strain relationship is linear with a large positive slope, indicating the elastic behavior. With increasing strain, the long period of the lamellar stacks increases in the stretching direction and decreases in the equatorial direction. The strain-induced melting (or crystal destruction) occurs in region II at a strain above 10%, where the stress−strain curve becomes nonlinear. In the initial stage of this region, the lamellar stacks perpendicular to the stretching direction melt faster than those aligned along the stretching direction.

2. In region III, new crystals with extended chain conformation start to form at 80% strain, which coincides with the yield point on the stress−strain curve. As the melting (destruction) process of the original crystals becomes dominant in this region, the engineering stress−strain relationship displays a slightly negative slope. At the yield point, the formation of elongated microvoids (craze) is formed.

3. Region IV starts at a strain around 120%, where the strain-induced melting is completed. In this region, the long period decreases and the scattered intensity increases with strain, indicating that the population of the strain-induced crystals increases. The stress−strain relationship shows a relatively small but positive slope.

4. During the relaxation, the majority of the strain-induced new crystals remain oriented. However, some induced crystals are reoriented with a decrease in strain, resulting in a weak four-point SAXS pattern. The recovery ratio of the EP copolymer is low, which is due to the formation of oriented new crystals that are thermally and mechanically stable. The microvoids can remain in the completely relaxed sample.

Acknowledgment. B.S.H. acknowledges the financial support by NSF (DMR-0098104). B.C. acknowledges the support by the Department of Energy (DEFG02-86ER 45237-016) and the U.S. Army Research Office (DAAD 190010419). The synchrotron beamline X27C was supported by the DoE (DEFG02-99ER 45760).

References and Notes

(1) Easterbrook, E. K.; Allen, R. D. Ethylene-Propylene Rubber. In *Rubber Technology*, 3rd ed.; Morton, M., Ed.; Kluwer Academic: Dordrecht, 1999; Chapter 9.
(2) Baldwin, F. P.; VerStrate, G. *Rubber Chem. Technol.* **1972**, *45*, 790.
(3) VerStrate, G.; Wilchinsky, Z. W. *J. Polym. Sci., Part A2* **1971**, *9*, 127.
(4) Sehanobish, K.; Patel, R. M.; Croft, B. A.; Chum, S. P.; Kao, C. I. *J. Appl. Polym. Sci.* **1994**, *51*, 887.
(5) Bensason, S.; Minick, J.; Moet, A.; Chum, S.; Hiltner, A.; Baer, E. *J. Polym. Sci., Polym. Phys.* **1996**, *34*, 1301.
(6) Geil, P. *Polymer Single Crystals*; Wiley-Interscience: New York, 1963.
(7) de Ballesteros, O. R.; Auriemma, F.; Guerra, G.; Corradini, P. *Macromolecules* **1996**, *29*, 7141.
(8) Guerra, G.; de Ballesteros, O. R.; Venditto, V.; Galimberti, M.; Sartori, F.; Pucciarello, R. *J. Polym. Sci., Part B: Polym. Phys.* **1999**, *37*, 1095.
(9) Kolbert, A. C.; Didier, J. G.; Xu, L. *Macromolecules* **1996**, *29*, 8591.
(10) Mathot, V. B. F.; Scherrenberg, R. L.; Pijipers, M. F. J.; Bras, W. *J. Therm. Anal.* **1996**, *46*, 681.
(11) Enderle, H. F.; Killian, H. G.; Hespe, H. *Colloid Polym. Sci.* **1986**, *264*, 305.
(12) Bonart, R.; Müller-Riederer, G. *Colloid Polym. Sci.* **1981**, *259*, 926.
(13) Bonart, R.; Hoffmann, K. *Colloid Polym. Sci.* **1984**, *262*, 1.
(14) Lin, S. B.; Hwang, K. S.; Tsay, S. Y.; Cooper, S. L. *Colloid Polym. Sci.* **1985**, *2*, 128.
(15) Shinzo, K.; Yuko, I.; Shinzo, Y.; Shibayama, M.; Tetsuo, K.; Shunji, N. *Polym. J.* **1991**, *23*, 991.

(16) Desper, C. R.; Schneider, N. S.; Jasinski, J. P.; Lin, J. S. *Macromolecules* **1985**, *18*, 2755.
(17) Shibayama, M.; Toshihito, K.; Tetsuo, K.; Shunji, N.; Takehisa, M. *Polym. J.* **1986**, *18*, 719.
(18) Tadokoro, H. *Structure of Crystalline Polymers*; Wiley-Interscience: New York, 1979.
(19) Brown, H. R.; Kramer, E. J. *J. Macromol. Sci., Phys.* **1981**, *B19*, 487.
(20) Brown, H. R.; Kramer, E. J.; Bubeck, R. A. *J. Mater. Sci.* **1988**, *23*, 248.

MA020771I